

Geometric interpretation of the hyperfine Breit–Rabi solution

Lihong V. Wang

Caltech Optical Imaging Laboratory
 Andrew and Peggy Cherng Department of Medical Engineering
 Department of Electrical Engineering
 California Institute of Technology
 1200 E. California Blvd., MC 138-78
 Pasadena, CA 91125, USA
 LVW@caltech.edu

September 16, 2025

Abstract

We present a geometric interpretation of the hyperfine Breit–Rabi eigenvalues and eigenvectors in alkali atoms after reformulating the standard solution into a compact form. In this picture, the nuclear magnetic moment has a polar angle fixed by the total projection quantum number. In contrast, the electron magnetic moment anti-aligns or aligns with an effective field formed by both the external magnetic flux density and the nuclear field, which simultaneously sets the mixing angle of the eigenvectors. This geometric view offers intuitive insight into the structure of the solutions.

Keywords hyperfine structure; Breit–Rabi; geometric interpretation; alkali atoms, quantum–classical correspondence

1 Introduction

The Breit–Rabi formula gives the dependence of hyperfine levels in atoms with a single valence electron on the magnetic flux density [1–3]. The derivation proceeds by diagonalizing the hyperfine Hamiltonian. Here, we recast the solution in a geometric form that resolves the roles of the electron and nuclear magnetic moments and clarifies how the total angular momentum quantum number F and the projection m_F quantize the relevant angles.

Figure 1 illustrates a canonical hyperfine Zeeman diagram for ${}^6\text{Li}$ with the nuclear spin quantum number $I = 1$. The Zeeman diagram displays the hyperfine energy levels of the system as a function of the applied magnetic flux density B . The top four levels constitute

the upper manifold, corresponding to the total angular momentum quantum number $F = \frac{3}{2}$, while the lower two levels form the lower manifold with $F = \frac{1}{2}$. Within the upper manifold, the two straight lines represent the stretched states, whereas oblique states refer to all other Zeeman sublevels. Each manifold converges to a single frequency or energy as $B \rightarrow 0$. An essential feature of the diagram is the mirror symmetry between the upper and lower manifolds in the oblique states. For $I = \frac{1}{2}, \frac{3}{2}$, see Appendices A and B, respectively.

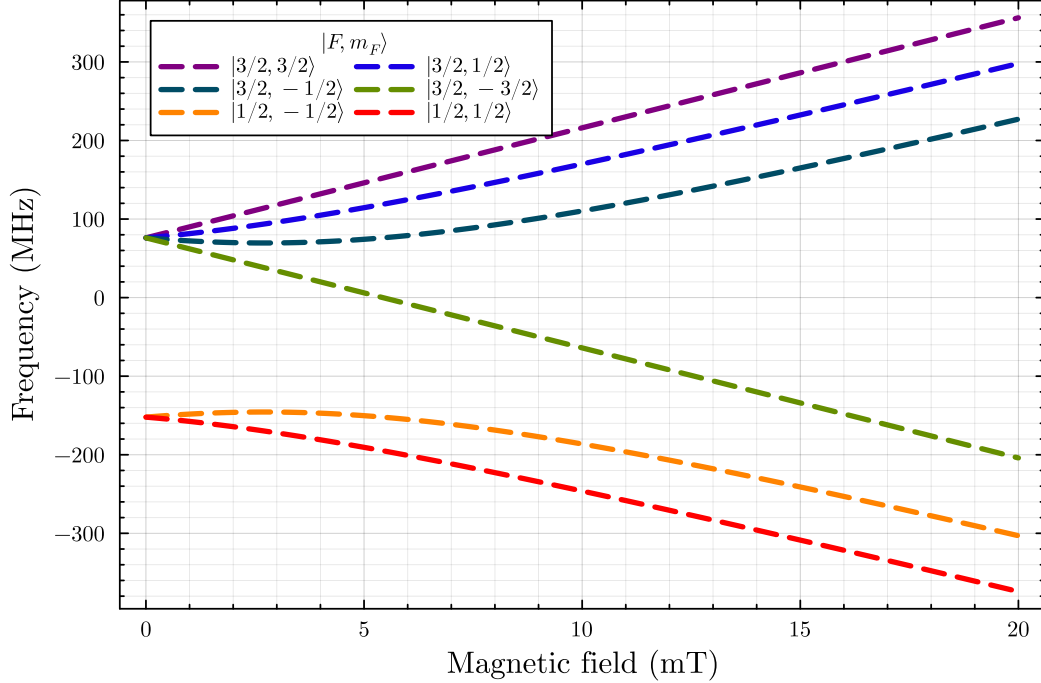


Figure 1: Hyperfine Zeeman structure of ${}^6\text{Li}$ with $I = 1$.

In the following, we first recapitulate the hyperfine Hamiltonian that governs the coupled electron–nuclear spin system, followed by the Breit–Rabi eigenstate solution in a finite field. We present a geometric interpretation of the Breit–Rabi solution, which provides intuitive insight into the underlying spin dynamics. Next, we geometrically represent the total angular momentum quantum numbers F and m_F in a vanishing field. A discussion follows, highlighting the physical implications of this picture. For completeness, we include in the appendices a recapitulated derivation of the Breit–Rabi solution and a reformulation of the associated mixing angle, as well as a reformulated Hamiltonian in Pauli form.

2 Hyperfine Hamiltonian

For an s -electron alkali atom in a static external magnetic flux density \mathbf{B} , the hyperfine Hamiltonian is

$$\hat{H} = -\hat{\boldsymbol{\mu}}_e \cdot \mathbf{B} - \hat{\boldsymbol{\mu}}_n \cdot \mathbf{B} + A \hat{\mathbf{S}} \cdot \hat{\mathbf{I}}, \quad (1)$$

where $\hat{\mathbf{S}}$ and $\hat{\mathbf{I}}$ are the dimensionless electron and nuclear spin operators with spin quantum numbers S and I , respectively; $\hat{\boldsymbol{\mu}}_e = \gamma_e \hbar \hat{\mathbf{S}}$ and $\hat{\boldsymbol{\mu}}_n = \gamma_n \hbar \hat{\mathbf{I}}$ are the electron and nuclear

magnetic moment operators; γ_e and γ_n are the corresponding gyromagnetic ratios; \hbar is the reduced Planck constant; and A is the hyperfine coupling constant. Here, $S = \frac{1}{2}$.

The total angular momentum operator is

$$\hat{\mathbf{F}} = \hat{\mathbf{S}} + \hat{\mathbf{I}}, \quad (2)$$

with $\hat{\mathbf{S}}$ and $\hat{\mathbf{I}}$ the electron and nuclear spin operators, respectively. The z -axis is taken along the direction of \mathbf{B} , i.e., $\mathbf{z} \parallel \mathbf{B}$.

In the limit of an infinitesimal magnetic flux density ($B \rightarrow 0$), where $B = |\mathbf{B}|$, the hyperfine Hamiltonian \hat{H} commutes with the total angular momentum squared,

$$[\hat{H}, \hat{\mathbf{F}}^2] \xrightarrow{B \rightarrow 0} 0. \quad (3)$$

Thus, the magnitude quantum number F is a good quantum number at $B = 0$ and an asymptotic good quantum number in this limit. We use the zero-field parent states F as adiabatic labels for the two branches at fixed m_F .

For any values of B , the Hamiltonian commutes with the z -component of the total angular momentum,

$$[\hat{H}, \hat{F}_z] = 0 \quad \forall B, \quad (4)$$

which implies that the projection quantum number m_F is always conserved.

3 Breit–Rabi eigenstate solution

The eigenenergies for $F = I \pm S \equiv F_{\pm}$ and projection m_F are derived for completeness in Appendix C [1–3]:

$$E_{\pm}(m_F, B) = -\frac{h\Delta\nu}{2(2I+1)} - \mu_N g_I m_F B \pm \frac{h\Delta\nu}{2} \sqrt{1 + \frac{2m_F x}{I+S} + x^2}. \quad (5)$$

where μ_N is the nuclear magneton and g_I is the nuclear g -factor. The dimensionless field parameter x is defined by

$$x \equiv -\frac{\hbar(\gamma_e - \gamma_n)B}{AF_+} = \frac{-g_e\mu_B + g_I\mu_N}{h\Delta\nu} B, \quad (6)$$

where μ_B is the Bohr magneton and $g_e < 0$, in our sign convention, is the electron g -factor. Because $-g_e\mu_B$ dominates, $x > 0$ for alkali atoms at $B > 0$. The zero-field hyperfine splitting energy determines the hyperfine coupling constant as follows:

$$h\Delta\nu = A(I+S), \quad (7)$$

where h is the Planck constant and $\Delta\nu$ is the frequency separation between the hyperfine levels at $B = 0$.

The signed magnitudes of the electron and nuclear magnetic moments are

$$\mu_e = \gamma_e S \hbar < 0, \quad \mu_n = \gamma_n I \hbar. \quad (8)$$

The electron gyromagnetic ratio is given by

$$\gamma_e = \frac{\mu_B g_e}{\hbar} < 0, \quad (9)$$

where the negative sign reflects the negative charge of the electron. The nuclear gyromagnetic ratio is

$$\gamma_n = \frac{\mu_N g_I}{\hbar}. \quad (10)$$

We consider only positive γ_n here because $\gamma_n > 0$ for most alkali nuclei.

The original Breit–Rabi eigenvalue formula ensures that the mean energy of all levels is set to zero. An alternative option shifts the energy levels so that the mean of all oblique levels vanishes:

$$E_{\pm}(m_F, B) = -\mu_N g_I m_F B \pm \frac{h\Delta\nu}{2} \sqrt{1 + \frac{2m_F x}{I + S} + x^2}. \quad (11)$$

The stretched states ($m_F = \pm F_+$) correspond to \mathbf{S} and \mathbf{I} being parallel, producing maximal total angular momentum in the upper manifold. The oblique states ($|m_F| < F_+$) refer to all other Zeeman sublevels and correspond to different orientations between \mathbf{S} and \mathbf{I} for nonzero B , resulting in a total angular momentum vector \mathbf{F} tilted relative to both spins.

Since the projection quantum number m_F is always conserved, for each fixed m_F and $S = \frac{1}{2}$, the relevant subspace is two-dimensional with the product basis

$$|+\rangle = |m_S = +\frac{1}{2}\rangle \otimes |m_I = m_F - \frac{1}{2}\rangle, \quad |-\rangle = |m_S = -\frac{1}{2}\rangle \otimes |m_I = m_F + \frac{1}{2}\rangle. \quad (12)$$

The normalized eigenvectors corresponding to E_{\pm} are

$$|\psi_{\pm}\rangle = \cos \frac{\alpha}{2} |\pm\rangle \pm \sin \frac{\alpha}{2} |\mp\rangle. \quad (13)$$

The mixing angle α is derived in Appendix D:

$$\tan \alpha = \frac{B_n \sin \theta}{\eta_{\gamma} B + B_n \cos \theta}, \quad (14)$$

where

$$\eta_{\gamma} \equiv 1 - \frac{\gamma_n}{\gamma_e} = 1 + \mathcal{O}\left(\frac{1}{1836}\right) \quad (15)$$

is introduced as a boost factor related to the gyromagnetic ratios for the electron Zeeman energy. Because the electron and nuclear gyromagnetic ratios differ by several orders of magnitude, the factor η_{γ} exceeds unity only slightly. When the angle α equals either 0 or π , we reach the stretched states, which are product states. In contrast, for other values of α , we obtain oblique states, which are entangled.

4 Geometric interpretation of the Breit–Rabi solution

In the zero-field limit, the eigenstates of the total angular momentum correspond to parallel ($F = I + S$) or antiparallel ($F = I - S$) coupling of the electron and nuclear magnetic moments. We introduce \mathbf{B}_n to denote the effective magnetic flux density pseudovector at the

electron produced by the nucleus; it is proportional to and parallel with the nuclear magnetic moment pseudovector $\boldsymbol{\mu}_n$ for an s -electron alkali atom via the Fermi-contact interaction [4, 5]. Therefore, the zero-field hyperfine splitting can be written as

$$h\Delta\nu = \Delta(-\boldsymbol{\mu}_e \cdot \mathbf{B}_n) = -2\mu_e B_n, \quad (16)$$

Similarly, one can write $h\Delta\nu = -2\mu_n B_e$. The quantity \mathbf{B}_e denotes the effective magnetic flux density pseudovector at the nucleus produced by the electron and is proportional to and parallel with the electron magnetic moment pseudovector $\boldsymbol{\mu}_e$.

The dimensionless field parameter can be rewritten as

$$x \equiv \frac{-\mu_B g_e + \mu_N g_I}{-2\mu_e} \frac{B}{B_n} \equiv \frac{\eta_\gamma B}{B_n}. \quad (17)$$

Next, we reformulate the standard Breit–Rabi eigenvalue formula to facilitate interpretation. By inspecting Eq. 11 after substitutions for $h\Delta\nu$ (Eq. 16) and x (Eq. 17), we observe that the square root term arises naturally from the cosine law. Accordingly, we define the polar angle θ such that

$$\cos \theta \equiv \frac{m_F}{I + S}. \quad (18)$$

Note that the denominator $I + S$ and the numerator $m_F \in [-(I + S), I + S]$ are for both the upper and lower manifolds, and one should not use $F = I - S$ or $\sqrt{(I + S)(I + S + 1)}$ [6] to determine θ . For now, this θ is a bookkeeping angle determined by m_F and the fixed scale $I + S$. We use it to cast energies in a compact cosine-law form.

Then, we also introduce a boost factor related to the angular momenta for the nuclear Zeeman energy

$$\eta_a = 1 + \frac{S}{I} \quad (19)$$

and an effective total field to be seen by the electron

$$\mathbf{B}_t = \eta_\gamma \mathbf{B} + \mathbf{B}_n, \quad B_t = \sqrt{(\eta_\gamma B)^2 + B_n^2 + 2(\eta_\gamma B) B_n \cos \theta}. \quad (20)$$

Consequently, Eq. 11 takes the compact form

$$E_{\pm} = -\mu_n \eta_a B \cos \theta \mp \mu_e B_t = -\boldsymbol{\mu}_n \cdot \eta_a \mathbf{B} - \boldsymbol{\mu}_e \cdot \mathbf{B}_t, \quad (21)$$

where the upper and lower signs correspond to the electron magnetic moment being antiparallel or parallel to \mathbf{B}_t as labeled by F_{\pm} . The first term on the right-hand side represents the nuclear Zeeman energy, where $\eta_n B$ is the effective field due to hyperfine coupling. The second term encompasses both the electron Zeeman energy and the hyperfine coupling energy. Now, it is clear that the polar angle θ determines that of the nuclear magnetic moment in the nuclear Zeeman contribution term, i.e., $\theta_n = \theta$, regardless of the external field or the eigenstate. While the full vector expectation $\langle \hat{\mathbf{I}} \rangle$ varies with the mixing angle α , this variation does not affect the term $-\mu_N g_I m_F B$.

The oblique states use m_F to set $\theta \neq 0$ or π , and the eigenenergies are split by $\pm \mu_e B_t$. In contrast, the stretched states with $m_F = \pm(I + S)$ have $\theta = 0$ or π , and the eigenenergies reduce to

$$E_{s\pm} = \mp(\mu_e + \mu_n)B - \mu_e B_n = \mp\mu_n B - \mu_e(\pm B + B_n). \quad (22)$$

Note that the boost factors have vanished. For the lower stretched state ($\theta = \pi$), we used $B_t = B_n - \eta_\gamma B$ at all field strengths when resolving the square root in Eq. 20.

Figure 2 presents a plausible geometric interpretation of the exact Breit–Rabi eigenvalue formula, summarizing the above observations. It is essential to note the constraint $\mathbf{B}_n \parallel \boldsymbol{\mu}_n$. The electron magnetic moment $\boldsymbol{\mu}_e$ is the only quantity that varies between the two eigenstates.

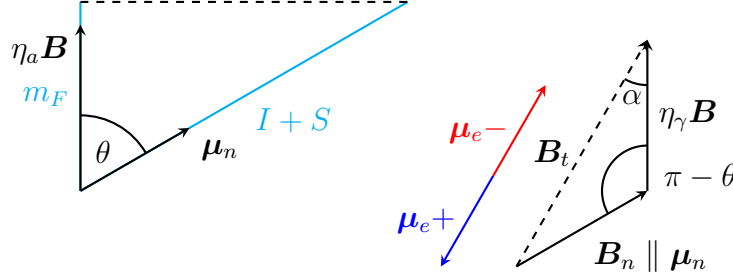


Figure 2: Geometric interpretation of the exact Breit–Rabi eigenenergies for a given m_F , where θ is set by m_F via $\cos \theta \equiv \frac{m_F}{I+S}$ (Eq. (18)) and α is the polar angle of \mathbf{B}_t via Eq. (14). The left triangle shows that the nuclear magnetic moment $\boldsymbol{\mu}_n$ has polar angle $\theta_n = \theta$, independent of the external field magnitude or the eigenstates $|\psi_+\rangle$ and $|\psi_-\rangle$ for a given m_F . The right triangle shows the two allowed orientations of the electron magnetic moment $\boldsymbol{\mu}_e$ relative to \mathbf{B}_t , pointing either against (+) or along (−) \mathbf{B}_t for eigenstates $|\psi_+\rangle$ and $|\psi_-\rangle$, i.e., its polar angle $\theta_e = \{\alpha, \pi + \alpha\}$ on the two-dimensional cross-section; it is the only quantity that varies between the two eigenstates. Alternatively, one can define the polar angle θ to lie within the interval $[0, \pi]$ and the azimuthal angle ϕ within $[0, 2\pi)$ to parameterize the two-sphere S^2 ; then, $\theta_e = \{\alpha, \pi + \alpha\}$ becomes $\theta_e = \{\alpha, \pi - \alpha\}$ paired with $\phi_e = \{0, \pi\}$.

The Hamiltonian block in the fixed- m_F two-dimensional subspace can be reformulated into Pauli form (see Appendix E):

$$H_{m_F} = -(\boldsymbol{\mu}_n \boldsymbol{\tau}_0) \cdot (\eta_a \mathbf{B}) - (\boldsymbol{\mu}_e \boldsymbol{\tau}) \cdot \mathbf{B}_t, \quad (23)$$

where $\boldsymbol{\tau}$ is the effective Pauli operator vector (Eq. 61). It is illuminating to compare the Hamiltonian in this representation with the reformulated eigenvalues given in Eq. 21, which we repeat below for convenience:

$$E_{\pm} = -\mu_n \eta_a B \cos \theta \mp \mu_e B_t = -\boldsymbol{\mu}_n \cdot (\eta_a \mathbf{B}) - \boldsymbol{\mu}_e \cdot \mathbf{B}_t. \quad (24)$$

We conclude that the first term represents the nuclear Zeeman contribution, while the second term incorporates both the electron Zeeman and hyperfine-interaction energies. Note that the eigenstates are the $\boldsymbol{\tau}$ -spinors parallel or antiparallel to $\mathbf{b} = -\boldsymbol{\mu}_e \mathbf{B}_t$:

$$\hat{\boldsymbol{\tau}} \cdot \mathbf{n}_e |\psi_{\pm}\rangle = \pm |\psi_{\pm}\rangle, \quad \mathbf{n}_e = \frac{\mathbf{b}}{|\mathbf{b}|}. \quad (25)$$

The effective field \mathbf{B}_t determines the mixing angle α , as shown in Appendix D; it also determines the direction of the electron magnetic moment (see Appendix E). Any pure state of a two-level system can be represented as a point on the Bloch sphere, with the two

orthonormal basis states conventionally located at the north and south poles. Therefore, the eigenvectors at a given m_F can be represented using the Bloch sphere (Fig. 3); in real space, the electron magnetic moment pseudovector is either anti-aligned or aligned with \mathbf{B}_t (see Appendix E).

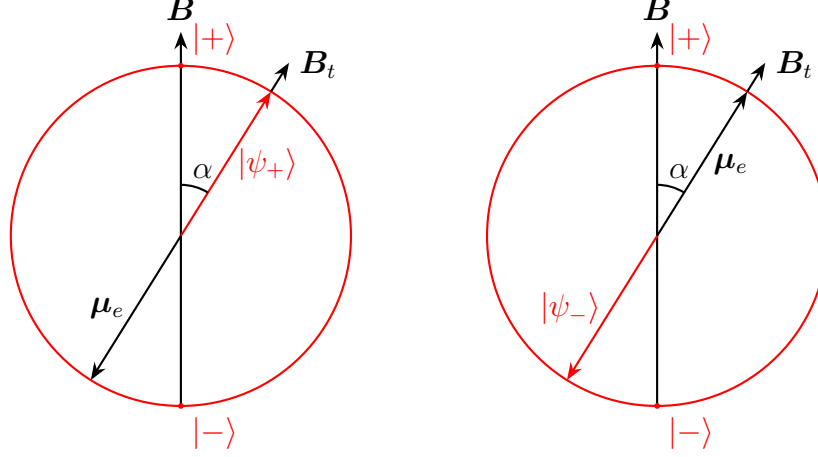


Figure 3: For the two-level subspace, Bloch-sphere representation of the exact Breit-Rabi eigenstates of \hat{H} at a given m_F (in red) and the real-space quantities from Fig. 2 associated with the eigenvalues (in black). Note that μ_e here points either against or along \mathbf{B}_t , i.e., its polar angle $\theta_e = \{\alpha, \pi + \alpha\}$ on the two-dimensional cross-section. Note that $|\pm\rangle = |m_S = \pm \frac{1}{2}\rangle \otimes |m_I = m_F \mp \frac{1}{2}\rangle$, $H_{m_F} = -\mu_n \tau_0 \cdot \eta_a \mathbf{B} - \mu_e \boldsymbol{\tau} \cdot \mathbf{B}_t$, $|\psi_{\pm}(m_F, B)\rangle = \cos \frac{\alpha}{2} |\pm\rangle \pm \sin \frac{\alpha}{2} |\mp\rangle$, and $E_{\pm}(m_F, B) = -\mu_n \eta_a B \cos \theta \mp \mu_e B_t = -\mu_n \cdot \eta_a \mathbf{B} - \mu_e \cdot \mathbf{B}_t$.

5 Geometric interpretation at $B \rightarrow 0$

In the limit $B \rightarrow 0$, F is an asymptotic good quantum number, and the allowed eigenstates are labeled by F and m_F , and the corresponding eigenstates admit a more straightforward geometric interpretation. Figure 4 illustrates the geometry of the total angular momentum $\mathbf{F} = \mathbf{S} + \mathbf{I}$ for ${}^6\text{Li}$ with nuclear spin $I = 1$ in the limit $B \rightarrow 0$. The polar angle of μ_n is determined by Eq. 18. The polar angle of \mathbf{B}_t

$$\lim_{x \rightarrow 0} \alpha = \theta. \quad (26)$$

The upper four configurations form the manifold with total angular momentum quantum number $F = \frac{3}{2}$, corresponding to the electron and nuclear spins \mathbf{S} and \mathbf{I} being aligned or their magnetic moments anti-aligned. In comparison, the lower two configurations constitute the manifold with $F = \frac{1}{2}$, which arises when \mathbf{S} and \mathbf{I} are oriented anti-aligned or their magnetic moments are aligned. Note that for the electron, the magnetic moment and the spin pseudovectors point in opposite directions due to the negative gyromagnetic ratio. Conversely, for the nucleus with a positive gyromagnetic ratio, the magnetic moment and the spin pseudovectors align in the same direction. See Appendices A and B for $I = \frac{1}{2}, \frac{3}{2}$, respectively. One may now introduce a field and vary it to rotate the electron magnetic moment μ_e adiabatically according to the right panel in Fig. 2.

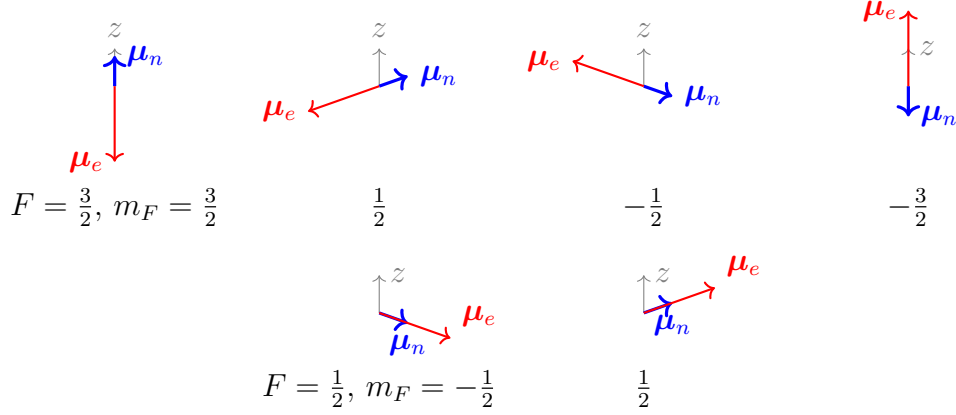


Figure 4: Geometric interpretation of the electron and nuclear magnetic moments for ${}^6\text{Li}$ with $I = 1$ in the limit $B \rightarrow 0$. The z axis is taken along the direction of the magnetic flux density \mathbf{B} . The polar angle of $\boldsymbol{\mu}_n$ is determined by Eq. 18, whereas the alignment of $\boldsymbol{\mu}_e$ with respect to $\boldsymbol{\mu}_n$ is determined by F . Due to the negative gyromagnetic ratio, the electron's magnetic moment points opposite to its spin pseudovector.

6 Discussion

The geometric interpretation indicates that the nuclear magnetic moment $\boldsymbol{\mu}_n$ is determined by the polar angle θ , independent of the external field \mathbf{B} , while the electron's magnetic moment aligns or anti-aligns with the effective field \mathbf{B}_t . As \mathbf{B} increases in magnitude slowly, \mathbf{B}_t changes accordingly, and the electron's magnetic moment $\boldsymbol{\mu}_e$ follows this field adiabatically. Stated differently, as the external field changes, \mathbf{B}_t changes, and $\boldsymbol{\mu}_e$ follows it adiabatically, while $\boldsymbol{\mu}_n$ remains stable at a given m_F . This asymmetry likely arises because the nuclear gyromagnetic ratio is orders of magnitude smaller, making nuclear spin precession much slower, while the electron spin rapidly adapts.

At $B = 0$, we label the eigenstates by $|F, m_F\rangle$ because $[\hat{H}, \hat{\mathbf{F}}^2] = 0$. For $B > 0$, the hyperfine and Zeeman terms do not commute with $\hat{\mathbf{F}}^2$, so F is not conserved. Nevertheless, m_F remains conserved for all B because of axial symmetry, and each fixed m_F subspace is at most two-dimensional for $S = \frac{1}{2}$. Turning on B slowly, the adiabatic theorem guarantees that a state initially in $|F_{\pm}, m_F\rangle$ evolves into the corresponding instantaneous eigenstate $E_{\pm}(m_F, B)$ without interbranch transitions. It is therefore natural to keep the zero-field F_{\pm} to label the two adiabatic branches for each m_F , which justifies calling F an adiabatic label; F itself is not conserved for $B > 0$. In particular, the stretched branches carry unique zero-field parents and remain unmixed as product states at all B . In contrast, the oblique branches are the adiabatic continuations of the F_+ and F_- parents, but they become mixtures of the two manifolds as entangled states as the field increases.

Even for protium (${}^1\text{H}$, $I = S$), the electron and nucleus behave asymmetrically, despite the apparent symmetry of the Hamiltonian. This asymmetry is likely rooted in the significant disparity between the electron and nuclear magnetic moments and their gyromagnetic ratios.

We will present the following discussions to encourage further investigation and dialogue. It is intended as a conceptual prompt rather than a definitive conclusion. Readers primarily interested in the main results may proceed to the next section.

The geometric interpretation, along with the above discussion, inspires the following adiabatic process to approximate the exact Breit–Rabi solution. Readers are referred to Fig. 1, Fig. 6, and Fig. 8 for guidance, and should follow the field strengths indicated below.

(1) Electron spin in \mathbf{B}_n without an external field ($B = 0$).

In the absence of an external field, the electron spin collapses to an eigenstate defined by the nuclear field \mathbf{B}_n . The Zeeman interaction Hamiltonian is

$$\hat{H}_e^{(0)} = -\gamma_e \hat{\mathbf{S}} \cdot \mathbf{B}_n. \quad (27)$$

Two hyperfine manifolds emerge as $F_+ = I + S$ and $F_- = I - S$.

(2) $\hat{\mathbf{F}}$ in an infinitesimally weak external field ($B \rightarrow 0$).

In the weak field regime where F remains an asymptotically good quantum number, the Zeeman interaction is well described by

$$\hat{H}_F = -\mu_B g_F \hat{\mathbf{F}} \cdot \mathbf{B}, \quad (28)$$

with g_F the hyperfine Landé factor. The angle θ of the quantized direction satisfies

$$\cos \theta = \frac{m_F}{I + S}, \quad (29)$$

which agrees with Eq. 18.

(3) Nuclear Zeeman energy in a finite-magnitude external field ($B \neq 0$) without re-quantization.

To quantify the nuclear Zeeman contribution, we define

$$\hat{H}_n = -\hat{\boldsymbol{\mu}}_n \cdot \mathbf{B} = -\gamma_n \hat{\mathbf{I}} \cdot \mathbf{B}. \quad (30)$$

However, we do not quantize the nuclear spin again; instead, we define its orientation by $\theta_n = \theta$, determined under $B \rightarrow 0$, which also orients $\mathbf{B}_n \parallel \boldsymbol{\mu}_n$.

(4) Electron spin in the total effective field \mathbf{B}_t .

When an external field is present, the electron spin is quantized along the total effective field \mathbf{B}_t . The corresponding interaction Hamiltonian is

$$\hat{H}_e = -\hat{\boldsymbol{\mu}}_e \cdot \mathbf{B}_t = -\gamma_e \hat{\mathbf{S}} \cdot \mathbf{B}_t. \quad (31)$$

This construction makes explicit that the electron senses both the applied field and the nuclear field. The slight deviation of η_γ in the expression of \mathbf{B}_t from unity due to hyperfine coupling might be related to the precessing \mathbf{B}_n ; thus, the natural quantization axis \mathbf{B}_t is not stationary.

(5) Total energy.

Collecting the contributions without double-counting the hyperfine coupling energy, we yield the following energy

$$E_\pm = -\mu_n B \cos \theta \mp \mu_e B_t = -\boldsymbol{\mu}_n \cdot \mathbf{B} - \boldsymbol{\mu}_e \cdot \mathbf{B}_t. \quad (32)$$

This equation reaches Eq. 21 if we set $\eta_a = 1$, which we found leads to only a minor error (typically $10^{-4} - 10^{-3}$) due to the much smaller nuclear Zeeman contribution to the total energy.

Through the hyperfine coupling, the electron and nuclear spins mutually dress each other, giving rise to the joint eigenstates of the Breit–Rabi Hamiltonian (see Appendix F). Within each fixed- m_F block, the nuclear Zeeman energy contribution boosted by η_a through hyperfine coupling, $-\eta_a \mu_n B \cos \theta$, depends only on $\cos \theta = m_F / (I + S)$, which is common to both eigenstates. While α depends on B , θ does not. A possible geometric picture treats the $\boldsymbol{\mu}_n$ as aligned with the quantization direction set by m_F ; in operator language, components transverse to \hat{F}_z do not affect the eigenenergy. Because the total angular momentum projection operator $\hat{F}_z = \hat{S}_z + \hat{I}_z$ determines the angle θ , the nuclear spin appears to follow the same projection and its Zeeman energy is boosted with $\frac{I+S}{I}$.

In the fixed- m_F subspace

$$\mathcal{H}_{m_F} = \text{span}\{|+\rangle, |-\rangle\}, \quad (33)$$

using $\hat{F}_z = \hat{S}_z + \hat{I}_z$ yields

$$\hat{F}_z |+\rangle = \hbar m_F |+\rangle, \quad \hat{F}_z |-\rangle = \hbar m_F |-\rangle, \quad (34)$$

hence

$$\hat{F}_z \Big|_{\mathcal{H}_{m_F}} = \hbar m_F \mathbf{1}. \quad (35)$$

For any normalized $|\psi\rangle \in \mathcal{H}_{m_F}$

$$\langle \psi | \hat{F}_z | \psi \rangle = \hbar m_F. \quad (36)$$

Thus, \hat{F}_z is proportional to the identity on \mathcal{H}_{m_F} , so any observable of the form $f(\hat{F}_z)$ cannot distinguish states within \mathcal{H}_{m_F} , consistent with the commutativity in Eq. 4. If the first Hamiltonian term depends only on \hat{F}_z , the dynamics and all expectation values coincide for all $|\psi\rangle \in \mathcal{H}_{m_F}$. In this restricted sense, the physics reduces effectively to a one-dimensional sector \mathbb{C}^1 , although the underlying Hilbert space remains two-dimensional \mathbb{C}^2 . Within the collapsed two-level subspace, the total angular momentum projection remains conserved, which permits treating the nuclear spin as a classical-like pseudovector.

Therefore, the eigenvectors of \hat{F}_z at a given m_F can be represented on a Bloch-sphere visualization of the fixed- m_F subspace, emphasizing that the nuclear Zeeman contribution depends only on θ ; the sphere itself is still the two-level space spanned by $\{|+\rangle, |-\rangle\}$ (Fig. 5). Here, the plus and minus basis vectors coincide in the same direction defined by a fixed polar angle θ . Regardless of the mixing angle α , the nuclear spin remains oriented in this direction. Strictly speaking, the full angular momentum operator $\hat{\mathbf{F}}$ determines the spin orientation, but within the fixed- m_F subspace \hat{F}_z already fixes the polar angle, and the transverse components provide no further distinction. Hence, it is sufficient to characterize the nuclear spin direction using \hat{F}_z alone in this context.

7 Conclusion

We presented a geometric interpretation of the Breit–Rabi energies. The total angular momentum used to quantize the angle θ is taken as $I + S$ for both the upper and lower manifolds. It establishes a uniform quantization reference for both hyperfine manifolds.

The quantized direction of the nuclear magnetic moment $\boldsymbol{\mu}_n$ is set by the angle θ regardless of the external field strength or the eigenstates at a given m_F , giving a scaled energy

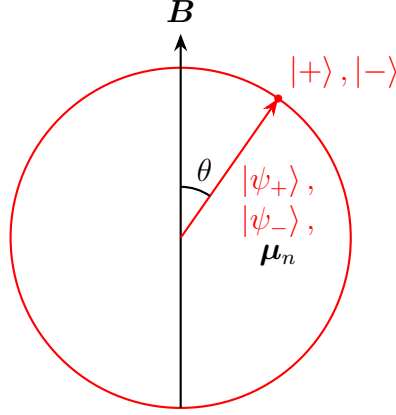


Figure 5: For the collapsed two-level subspace, Bloch-sphere representation of the Breit-Rabi eigenstates of \hat{F}_z at a given m_F (in red) and the real-space quantities including μ_n in the dressed state from Fig. 2 associated with the eigenvalues (in black). Note that $\cos \theta \equiv \frac{m_F}{I+S}$, $|\pm\rangle = |m_S = \pm \frac{1}{2}\rangle \otimes |m_I = m_F \mp \frac{1}{2}\rangle$, $H_{m_F} = -\mu_n \tau_0 \cdot \eta_a \mathbf{B} - \mu_e \boldsymbol{\tau} \cdot \mathbf{B}_t$, $|\psi_{\pm}(m_F, B)\rangle = \cos \frac{\alpha}{2} |\pm\rangle \pm \sin \frac{\alpha}{2} |\mp\rangle$, and $E_{\pm}(m_F, B) = -\mu_n \eta_a B \cos \theta \mp \mu_e B_t = -\mu_n \cdot \eta_a \mathbf{B} - \mu_e \cdot \mathbf{B}_t$.

$-(1 + \frac{S}{I}) \mu_n B \cos \theta$. This expression reflects the effective coupling of the nuclear magnetic moment to the applied field, providing a simple geometric picture for the nuclear contribution to the total energy.

For the electron magnetic moment μ_e , the quantization is taken against or along the total effective field $\mathbf{B}_t = \eta_\gamma \mathbf{B} + \mathbf{B}_n$, where $\eta_\gamma = 1 - \frac{\gamma_n}{\gamma_e} = 1 + \mathcal{O}(\frac{1}{1836})$. The effective field also sets the mixing angle of the eigenvectors. The resulting energy term $\mp \mu_e B_t$ incorporates both the applied field and the internal field from the nucleus. As one varies the external field, the electron's magnetic moment follows the effective field adiabatically, consistent with larger level splittings and faster Larmor precession for the electron; adiabaticity holds when the field is ramped slowly compared to the instantaneous eigenenergy gap. The $\frac{\gamma_n}{\gamma_e}$ factor in η_γ due to hyperfine coupling may be related to the precessing quantization axis \mathbf{B}_t .

8 Acknowledgments

The author thanks Kelvin Titimbo for providing the Zeeman diagrams (Figures 1, 6, and 8) and thanks our team members—Kelvin Titimbo, Suleyman Kahraman, Xukun Lin, Qihang Liu, Mark Zhu, and Arthur Chang—for their helpful discussions.

References

- [1] G. Breit and I. I. Rabi, “Measurement of nuclear spin”, *Physical Review* **38**, 2082 (1931).
- [2] I. I. Rabi, “On the process of space quantization”, *Physical Review* **49**, 324 (1936).
- [3] P. Kusch, S. Millman, and I. I. Rabi, “The radiofrequency spectra of atoms: hyperfine structure and zeeman effect in the ground state of ^6Li , ^7Li , ^{39}K , and ^{41}K ”, *Physical Review* **57**, 765–780 (1940).

- [4] M. Bucher, “The electron inside the nucleus: an almost classical derivation of the isotropic hyperfine interaction”, *European Journal of Physics* **21**, 19 (2000).
- [5] L. V. Wang, “Multi-stage Stern–Gerlach experiment modeled”, *Journal of Physics B: Atomic, Molecular and Optical Physics* **56**, 105001 (2023).
- [6] R. P. Feynman, R. B. Leighton, and M. Sands, *The Feynman Lectures on Physics, Vol. III* (Addison-Wesley, 2005), Ch. 34–7, p. A–11.

A Zeeman diagram and geometry for ^1H , $I = 1/2$

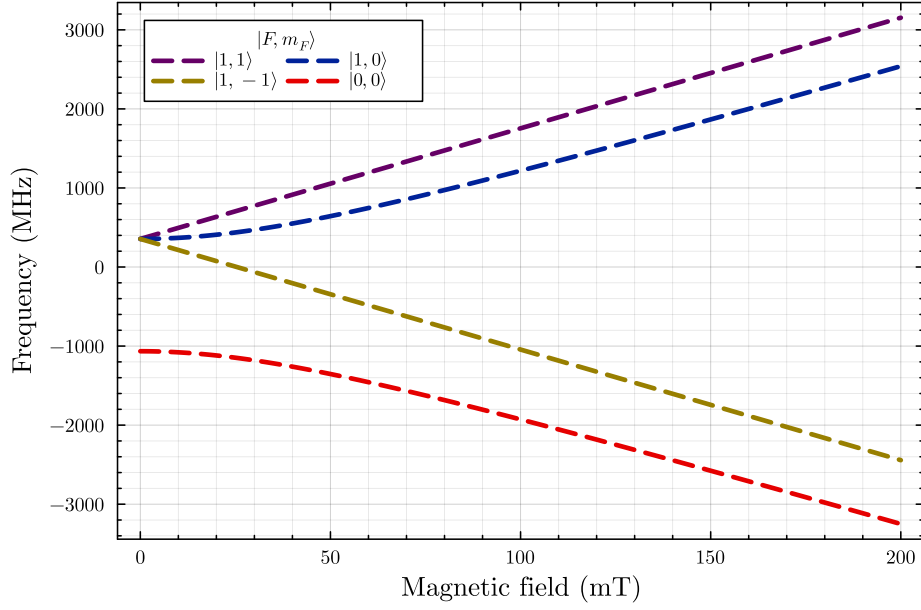


Figure 6: Hyperfine Zeeman structure of ^1H with $I = \frac{1}{2}$.

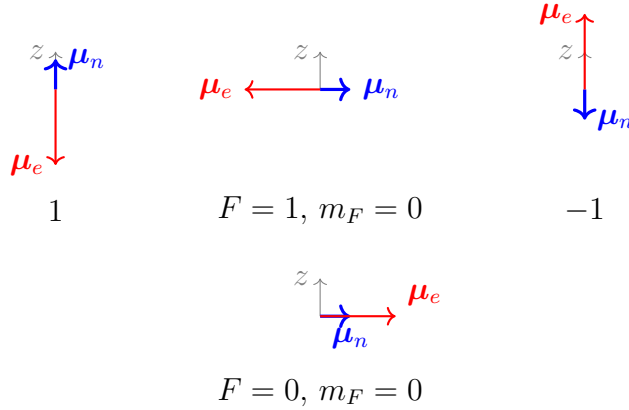


Figure 7: Geometric interpretation of the electron and nuclear magnetic moments for ^1H with $I = \frac{1}{2}$ in the limit $B \rightarrow 0$. The z axis is taken along the direction of the magnetic flux density \mathbf{B} .

B Zeeman diagram and geometry for ^{39}K , $I = 3/2$

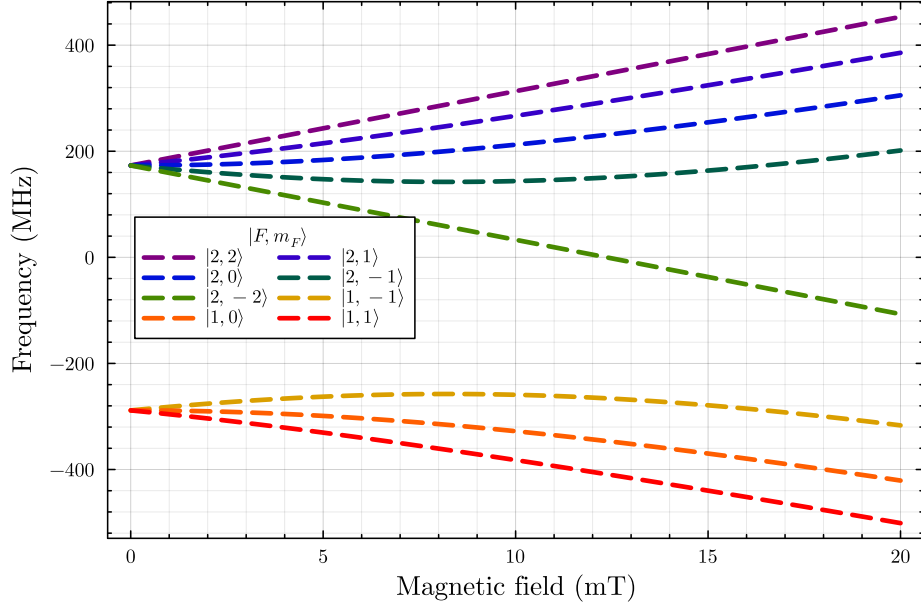


Figure 8: Hyperfine Zeeman structure of ^{39}K with $I = \frac{3}{2}$.

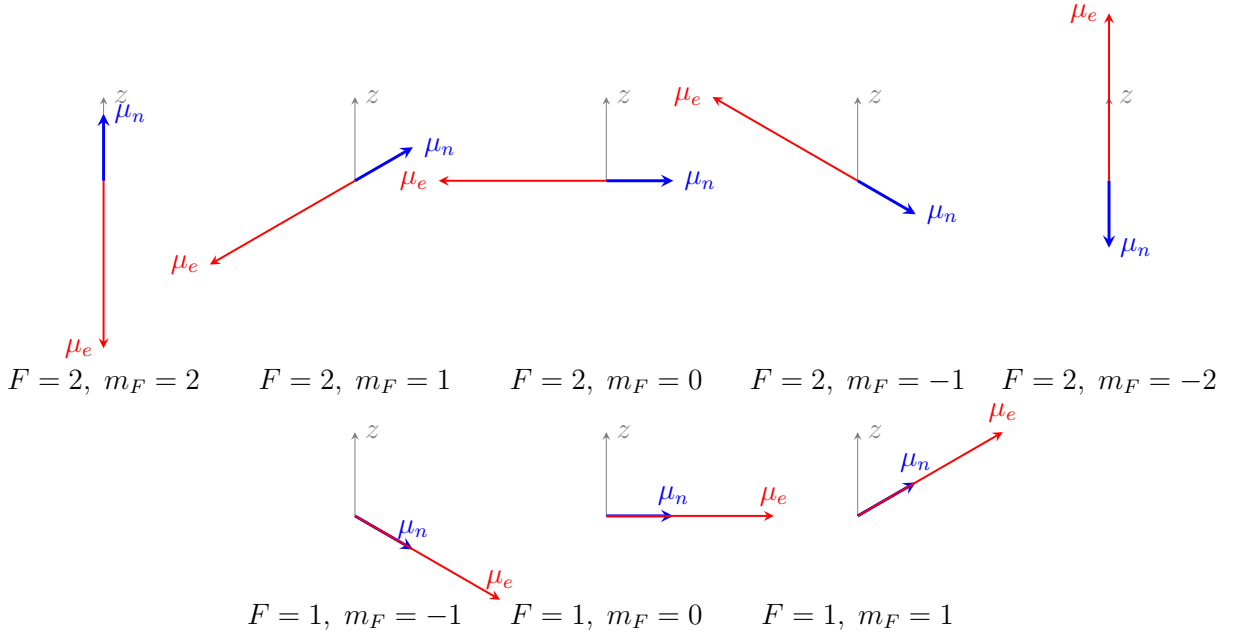


Figure 9: Geometric interpretation of the electron and nuclear magnetic moments for ^{39}K with $I = \frac{3}{2}$ in the limit $B \rightarrow 0$. The z axis is taken along the direction of the magnetic flux density \mathbf{B} .

C Derivation of the Breit–Rabi solution

C.1 Hamiltonian and two-state basis

We consider an alkali atom with electron spin $S = \frac{1}{2}$ and nuclear spin I in a static field of magnitude B along the laboratory z axis. The Zeeman and hyperfine Hamiltonian reads

$$\hat{H} = -\hbar B(\gamma_e \hat{S}_z + \gamma_n \hat{I}_z) + A\left(\hat{S}_z \hat{I}_z + \frac{1}{2}(\hat{S}_+ \hat{I}_- + \hat{S}_- \hat{I}_+)\right). \quad (37)$$

We use $\gamma_e = g_e \mu_B / \hbar$ and $\gamma_n = g_I \mu_N / \hbar$ with $g_e < 0$. The subscripts $+$ and $-$ denote the ladder operators, with $+$ indicating raising and $-$ indicating lowering. The total magnetic quantum number $m_F = m_S + m_I$ is conserved.

For each fixed m_F and $S = \frac{1}{2}$, the relevant subspace is two-dimensional with the product basis

$$|+\rangle = |m_S = +\frac{1}{2}\rangle \otimes |m_I = m_F - \frac{1}{2}\rangle, \quad |-\rangle = |m_S = -\frac{1}{2}\rangle \otimes |m_I = m_F + \frac{1}{2}\rangle. \quad (38)$$

We now restrict our attention to each subspace corresponding to a fixed m_F .

C.2 Matrix elements

The diagonal matrix elements follow from (37) because $\hat{S}_+ \hat{I}_- + \hat{S}_- \hat{I}_+$ has no diagonal contribution in the product basis

$$H_{++} = -\hbar B\left(\gamma_e \frac{1}{2} + \gamma_n(m_F - \frac{1}{2})\right) + A\left(\frac{1}{2}(m_F - \frac{1}{2})\right), \quad (39)$$

$$H_{--} = +\hbar B\left(\gamma_e \frac{1}{2} - \gamma_n(m_F + \frac{1}{2})\right) - A\left(\frac{1}{2}(m_F + \frac{1}{2})\right). \quad (40)$$

The off-diagonal elements arise from the flip-flop term. Using the standard ladder matrix elements,

$$\hat{S}_+ |S, m_S\rangle = \sqrt{(S - m_S)(S + m_S + 1)} |S, m_S + 1\rangle, \quad (41)$$

$$\hat{I}_- |I, m_I\rangle = \sqrt{(I + m_I)(I - m_I + 1)} |I, m_I - 1\rangle, \quad (42)$$

one obtains the equal off-diagonal elements as

$$\begin{aligned} \chi &\equiv H_{+-} = H_{-+} \\ &= \frac{A}{2} \langle S, +\frac{1}{2} | \hat{S}_+ | S, -\frac{1}{2} \rangle \langle I, m_F - \frac{1}{2} | \hat{I}_- | I, m_F + \frac{1}{2} \rangle \\ &= \frac{A}{2} \sqrt{(I + \frac{1}{2})^2 - m_F^2}. \end{aligned} \quad (43)$$

For stretched states, $\chi = 0$.

For convenience, we define the mean and half-difference of the diagonal elements as

$$M \equiv \frac{H_{++} + H_{--}}{2}, \quad d \equiv \frac{H_{++} - H_{--}}{2}. \quad (44)$$

With (39)–(40), one finds

$$M = -\hbar \gamma_n m_F B - \frac{A}{4}, \quad d = -\frac{\hbar}{2}(\gamma_e - \gamma_n)B + \frac{A}{2}m_F. \quad (45)$$

Note that d is related to the two Larmor frequencies.

C.3 Eigenvectors and eigenvalues

The eigenvalue equation satisfied by the eigenvectors $|\psi_{\pm}\rangle$ and eigenvalues E_{\pm} is

$$\hat{H}_{m_F} |\psi_{\pm}\rangle = E_{\pm} |\psi_{\pm}\rangle. \quad (46)$$

The Hamiltonian \hat{H}_{m_F} is expressed in the $\{|+\rangle, |-\rangle\}$ basis as the Hamiltonian matrix

$$H_{m_F} = \begin{pmatrix} H_{++} & \chi \\ \chi & H_{--} \end{pmatrix}. \quad (47)$$

We define a mixing angle α via

$$\tan \alpha \equiv \frac{\chi}{d}. \quad (48)$$

The normalized eigenvectors are

$$|\psi_{\pm}\rangle = \cos \frac{\alpha}{2} |\pm\rangle \pm \sin \frac{\alpha}{2} |\mp\rangle. \quad (49)$$

The corresponding eigenvalues are

$$E_{\pm} = M \pm \sqrt{d^2 + \chi^2} = \frac{H_{++} + H_{--}}{2} \pm \frac{1}{2} \sqrt{(H_{++} - H_{--})^2 + 4\chi^2}. \quad (50)$$

Introduce $F_+ \equiv I + S$ and define the dimensionless field parameter x (Eq. 17) by

$$x \equiv -\frac{\hbar(\gamma_e - \gamma_n)B}{AF_+} = \frac{-g_e\mu_B + g_I\mu_N}{h\Delta\nu} B, \quad h\Delta\nu = AF_+. \quad (51)$$

Using (43), (45), and (51) in (50), and recalling $\hbar\gamma_n = \mu_N g_I$ (Eq. 10), one obtains the Breit–Rabi form:

$$E_{\pm}(m_F, B) = -\frac{h\Delta\nu}{2(2I+1)} - \mu_N g_I m_F B \pm \frac{h\Delta\nu}{2} \sqrt{1 + \frac{2m_F x}{I+S} + x^2}. \quad (52)$$

The constant offset $-h\Delta\nu/[2(2I+1)]$ can be dropped without affecting energy spacings or eigenvectors.

D Reformulation of the mixing angle

Introduce the geometric angle θ via Eq. 18

$$\cos \theta = \frac{m_F}{F_+}, \quad \sin \theta = \sqrt{1 - \left(\frac{m_F}{F_+}\right)^2}. \quad (53)$$

Using (43)–(45), one gets

$$2\delta = H_{++} - H_{--} = AF_+(x + \cos \theta), \quad 2\chi = AF_+ \sin \theta. \quad (54)$$

Substitution into (48) gives the compact relation

$$\tan \alpha = \frac{\sin \theta}{x + \cos \theta}. \quad (55)$$

Using Eq. 17

$$x \equiv \frac{\eta_\gamma B}{B_n}, \quad (56)$$

we obtain

$$\tan \alpha = \frac{B_n \sin \theta}{\eta_\gamma B + B_n \cos \theta}. \quad (57)$$

Therefore, the angle α is the polar angle of \mathbf{B}_t measured from the $+z$ axis.

Note that

$$\lim_{x \rightarrow 0} \alpha = \theta. \quad (58)$$

Substituting $\alpha \rightarrow \theta$ into (49) gives the Clebsch–Gordan limit:

$$|\psi_+(m_F, 0)\rangle = \cos \frac{\theta}{2} |+\rangle + \sin \frac{\theta}{2} |-\rangle = \sqrt{\frac{F_+ + m_F}{2F_+}} |+\rangle + \sqrt{\frac{F_+ - m_F}{2F_+}} |-\rangle, \quad (59)$$

$$|\psi_-(m_F, 0)\rangle = -\sin \frac{\theta}{2} |+\rangle + \cos \frac{\theta}{2} |-\rangle = -\sqrt{\frac{F_+ - m_F}{2F_+}} |+\rangle + \sqrt{\frac{F_+ + m_F}{2F_+}} |-\rangle. \quad (60)$$

Equation (55) together with (49) ensures that the eigenvectors are the electron spinors aligned and anti-aligned with the effective field \mathbf{B}_t of (20). The stretched states at $m_F = \pm F_+$ satisfy $\sin \theta = 0$ and $\chi = 0$, hence $\alpha \rightarrow 0$ or π , and both $|\psi_+\rangle$ and $|\psi_-\rangle$ reduce to the unmixed product states at the edges, which confirms internal consistency.

E Reformulation of the Hamiltonian into Pauli form

In the fixed- m_F two-dimensional subspace $\mathcal{H}_{m_F} = \text{span}\{|+\rangle, |-\rangle\}$, we define effective Pauli operators (including the identity)

$$\begin{aligned} \hat{\tau}_x &= |+\rangle\langle -| + |-\rangle\langle +|, \\ \hat{\tau}_y &= -i(|+\rangle\langle -| - |-\rangle\langle +|), \\ \hat{\tau}_z &= |+\rangle\langle +| - |-\rangle\langle -|, \\ \hat{\tau}_0 &= |+\rangle\langle +| + |-\rangle\langle -|. \end{aligned} \quad (61)$$

The operators act only within this reduced space and should be clearly distinguished from the physical electron Pauli operators $\hat{\sigma}_i$, acting on the physical electron spin space spanned by $\{|m_s = +\frac{1}{2}\rangle, |m_s = -\frac{1}{2}\rangle\}$. The four effective Pauli matrices are

$$\tau_0 = \begin{pmatrix} 1 & 0 \\ 0 & 1 \end{pmatrix}, \quad \tau_x = \begin{pmatrix} 0 & 1 \\ 1 & 0 \end{pmatrix}, \quad \tau_y = \begin{pmatrix} 0 & -i \\ i & 0 \end{pmatrix}, \quad \tau_z = \begin{pmatrix} 1 & 0 \\ 0 & -1 \end{pmatrix}. \quad (62)$$

Recall the Hamiltonian matrix in the constant- m_F two-dimensional subspace

$$H_{m_F} = \begin{pmatrix} H_{++} & \chi \\ \chi & H_{--} \end{pmatrix} = \begin{pmatrix} M + d & \chi \\ \chi & M - d \end{pmatrix}. \quad (63)$$

It is convenient to recast the Hamiltonian into Pauli form. Introducing the vector

$$\mathbf{b} = (\chi, 0, d), \quad (64)$$

one obtains

$$H_{m_F} = M \tau_0 + \mathbf{b} \cdot \boldsymbol{\tau}. \quad (65)$$

The vector \mathbf{b} plays the role of a fictitious field, up to a constant factor, and turns out to be \mathbf{B}_t . Its direction defines the sharp axis of the electron spin

$$\mathbf{n}_e = \frac{\mathbf{b}}{|\mathbf{b}|} = (\sin \alpha, 0, \cos \alpha), \quad \tan \alpha = \frac{\chi}{d}. \quad (66)$$

Diagonalization of the Hamiltonian is therefore immediate: the eigenvalues are $E_{\pm} = M \pm |\mathbf{b}|$, with eigenvectors $|\psi_{\pm}\rangle$ aligned or anti-aligned with \mathbf{n}_e . While the term M gives the nuclear Zeeman energy, the term $\pm |\mathbf{b}|$ gives the electron Zeeman energy and the hyperfine coupling energy.

From Eq. 45 and Eq. 21, we find

$$M = -\boldsymbol{\mu}_n \cdot \eta_a \mathbf{B}, \quad (67)$$

apart from a constant energy shift. Similarly, we have

$$\mathbf{b} = -\mu_e \mathbf{B}_t. \quad (68)$$

Therefore, we obtain

$$H_{m_F} = -(\boldsymbol{\mu}_n \tau_0) \cdot (\eta_a \mathbf{B}) - (\mu_e \boldsymbol{\tau}) \cdot \mathbf{B}_t. \quad (69)$$

F Dressed-state analogy of the Breit–Rabi block

A dressed state is an eigenstate of the interacting system that includes both the matter degrees of freedom and the coupling that mixes the relevant bare states. The matter degrees of freedom are the bare hyperfine basis states $|m_s, m_I\rangle$, built from the electron spin S and nuclear spin I . The interaction that mixes these bare states is the hyperfine flip–flop term, together with the Zeeman shifts that produce differential energies for the basis states. The resulting dressed state is therefore a coherent superposition of two bare configurations at fixed $m_F = m_s + m_I$.

In a fixed- m_F subspace spanned by $\{|+\rangle, |-\rangle\}$, the Hamiltonian can be written in Pauli form $H_{m_F} = M \tau_0 + d \tau_z + \chi \tau_x$ with the effective field $\mathbf{b} = (\chi, 0, d)$, $|\mathbf{b}| = \sqrt{d^2 + \chi^2}$.

For comparison, a driven two-level system in the rotating frame under the rotating-wave approximation has

$$H_{\text{RWA}} = \frac{\hbar}{2} (-\Delta \sigma_z + \Omega \sigma_x), \quad \Omega_R = \sqrt{\Delta^2 + \Omega^2}. \quad (70)$$

The following parameter map identifies the two problems

$$d = -\frac{\hbar}{2} \Delta, \quad \chi = \frac{\hbar}{2} \Omega, \quad |b| = \frac{\hbar}{2} \Omega_R, \quad (71)$$

while the scalar offset $M \tau_0$ only shifts both energies equally and does not affect splittings within the constant- m_F subspace.

The term $d \tau_z$ plays the role of a detuning inside the fixed- m_F block. The term $\chi \tau_x$ is the coherent coupling that mixes the two bare states. In an alkali hyperfine manifold, χ originates from the flip-flop part of the contact hyperfine interaction $\frac{A}{2}(S_+ I_- + S_- I_+)$. The vector \mathbf{b} is the Bloch-vector representation of the effective field that sets the quantization axis for the spinor.